# Spatial recurrence plots

D. B. Vasconcelos, S. R. Lopes, and R. L. Viana
*Departamento de Física, Universidade Federal do Paraná, 81531-990, Curitiba, Paraná, Brazil*

J. Kurths
*Institut für Physik, Universität Potsdam, PF 601553, D-14415, Potsdam, Germany*

(Received 3 June 2005; revised manuscript received 17 February 2006; published 23 May 2006)

We propose an extension of the recurrence plot concept to perform quantitative analyzes of roughness and disorder of spatial patterns at a fixed time. We introduce spatial recurrence plots (SRPs) as a graphical representation of the pointwise correlation matrix, in terms of a two-dimensional spatial return plot. This technique is applied to the study of complex patterns generated by coupled map lattices, which are characterized by measures of complexity based on SRPs. We show that the complexity measures we propose for SRPs provide a systematic way of investigating the distribution of spatially coherent structures, such as synchronization domains, in lattice profiles. This approach has potential for many more applications, e.g., in surface roughness analyzes.

DOI: 10.1103/PhysRevE.73.056207 PACS number(s): 05.45.Xt, 05.45.Jn, 05.45.Ra

## I. INTRODUCTION

Recurrence plots (RPs) have been introduced as a numerical tool to calculate the maximum Lyapunov exponent related to a time series [1]. Later it was shown that RPs can also be used to study the nonstationarity of a time series as well as to indicate its degree of aperiodicity [2]. Many time series obtained from experiments and theoretical models are nonstationary due to the existence of multiple time scales [3]. The basic idea of a RP is to start from a phase space embedding (using delay coordinates, for example) and compare the embedding vectors with each other, drawing pixels when the Euclidean distance between vectors is below some threshold. In other words, RPs are graphical representations of the correlation matrix for time-delayed phase points [4].

As an example, stationary time series yield RPs which are homogeneous along a diagonal line. Moreover, if the RP shows a cloud of points with a homogeneous yet irregular distribution, then the time series has a pronounced stochastic nature. On the other hand, the formation of patterns in RPs may indicate stationary chaotic behavior. Recurrence plots have been extensively used for a wide variety of applications, such as to recover smooth dynamics from time series [5,6], measure complex behavior in heart-rate-variability data [7], fluid dynamics [8], electroencephalographic data [9], and noise reduction [10,11].

Since RPs have been found so useful on characterizing complex dynamics in the time domain, their extension to the spatial domain—the characterization of spatial order and disorder—would be a welcome addition to the toolbox of nonlinear dynamics. In particular, spatial recurrence plots (SRPs) can shed some more light on the outstanding problem of how to characterize spatiotemporal chaos, regarded here as the loss of spatial and temporal correlations in different scales [12].

In this paper we propose an extension of RPs to spatial systems by considering space-separated vectors obtained from a given spatial pattern at a fixed time. Spatial return properties of lattice coupled systems have been studied [13,14], but an approach via RP has not been done so far. As a prototype of a class of spatially extended dynamical systems we consider coupled map lattices (CMLs). Here we use the discreteness of CMLs as a natural way to consider spatially separated vectors, in a straightforward application of the embedding technique [16]. Spatially disordered one-dimensional patterns stemming from chaotic deterministic systems can be numerically produced as the output of a lattice of coupled logistic maps, for example. Sinha has investigated the influence of parametric noise on the spatially homogeneous phase of a generalized coupled map lattice with varying ranges of interaction [17].

A lattice of coupled chaotic maps is able to generate complex profiles consisting of a spatially disordered region coexisting with spatially homogeneous plateaus, which is just the kind of situation for which we claim SRPs are useful. In this sense the CML model considered in this paper is paradigmatic. Moreover, if we have in mind that many numerical schemes for integration of partial differential equations (PDEs) resort to space and time discretizations, results obtained for coupled map lattices are also of potential interest for PDEs.

We claim that SRPs can be used to distinguish different kinds of disordered spatial patterns. As we will see, SRP provides a way to detect and quantify the existence of spatially coherent domains coexistent with disordered regions. Usual methods of analyses do not always cope with these kind of spatially complex patterns, since they focus on gross features of the pattern, rather than on the details of the coherent domains. One of the most widely applied measures of profile roughness is the interface width, defined for a one-dimensional profile $h(i)$, $i=1,2,\ldots,N$ being the discrete spatial index, as the rms fluctuation in the height $h$ at fixed time [18] $w(N)=\{\frac{1}{N}\Sigma_{i=1}^{N}[h(i)-\langle h\rangle]^2\}^{1/2}$, where $\langle h\rangle=(1/N)\Sigma_{i=1}^{N}h(i)$ is the average height of the profile. The interface width quantifies the profile smoothness degree, but it smears out the pattern irregularities, overlooking possibly existent spatially

 

coherent domains. This is also a shortcoming of statistical treatments based on a height-height correlation function, which provides a good description of self-affine profiles, such as those found in brittle fracture profiles [19]; and for which the corresponding Hurst exponent was found to take on a universal value [20].

In addition, techniques based on spatial Fourier transform, while being linear procedures, may not work properly for spatial profiles generated deterministically by a nonlinear process. Moreover, Fourier transforms are very sensitive to noise in that spurious peaks may appear in the spectra of complex profiles. For example, if one performs a spatial Fourier analysis of a profile consisting of regular plateaus mixed with irregular domains, we can resolve only some "wave vector" peaks, without any information about the length and number of spatially coherent plateaus. In SRPs, on the contrary, those plateaus are directly linked to the vertical and/or horizontal structures; and accordingly we use quantitative diagnostics such as the laminarity and trapping length in order to characterize such a complex spatial profile. The difficulties pointed out for Fourier techniques are not likely to disappear if other techniques, e.g., wavelets, are used.

Another advantage of the spatial recurrence analysis is the possibility it opens to distinguish between spatial profiles generated by random processes, as in the Kardar-Parisi-Zhang equation [21], from those obtained as a result of chaotic space-time dynamics. For the latter we choose a coupled lattice of chaotic maps, since it became a paradigmatic example of spatially extended systems and a useful benchmark where techniques such as SRPs can be tested before their use in more complicated systems. We foresee potential applications of the SRP technique in various fields, especially in the surface roughness analyses applied to situations such as flowing sand patterns [22], semiconductor interfaces [23], friction reduction [24], and sea-floor microtopography [25], among many others.

The paper is organized as follows. In the second section we describe the CML to be studied and the basic ideas underlying spatial embeddings at a fixed time. Such an embedding furnishes space-separated vectors, from which a spatial correlation integral can be computed. Section III introduces SRPs from space-separated vectors and presents quantitative characterizations of spatial randomness based on symmetric structures found in the plots. The last section contains our conclusions.

## II. SPATIAL EMBEDDING FOR A LATTICE-COUPLED DYNAMICAL SYSTEM

Coupled map lattices are spatially extended systems with discrete time and space, but allowing a continuous state variable attached to each lattice site, satisfying a given dynamical process [26]. They have been extensively used for more than two decades, thanks to the fact that many features, common to spatially extended systems, are already present in CMLs; but can be observed with considerable saving of computer time, when compared to partial differential equations, for example Ref. [27].

One particular advantage of CMLs is their flexibility to cope with one's needs of simulating particularly interesting spatio-temporal patterns. For instance, much work has been done in logistic map lattices with local (diffusive) interactions, for which only the nearest-neighbor sites are coupled to a given map [28]. However, the resulting phase diagram is rather sensitive to variations of the nonlinearity parameter. Hence we shall take the extreme case of a logistic map at outer crisis, where the local dynamics is the most chaotic, and use a flexible coupling scheme. This also includes long-range interactions such that the coupling strength decreases with the lattice distance in a power-law fashion [29].

Accordingly, the CML model to be used in this paper to generate spatially disordered patterns, consists of a one-dimensional chain of $N$ sites labeled by the superindex $i=0,1,\ldots,N-1$. At each site a dynamical variable at time $n$, $x_n^{(i)}$, evolves in time according to a discrete process $x \mapsto f(x)=4x(1-x)$, where $x \in [0,1]$, for which the uncoupled maps display strongly chaotic behavior with Lyapunov exponent $\lambda_U=\ln 2$. The nonlocal form of coupling to be dealt with in this paper is

$$x_{n+1}^{(i)} = (1-\epsilon) f(x_n^{(i)}) + \frac{\epsilon}{\eta(\alpha)} \sum_{j=1}^{N'} \frac{1}{j^\alpha} [f(x_n^{(i+j)}) + f(x_n^{(i-j)})], \quad (1)$$

where $\epsilon > 0$ and $\alpha > 0$ are the coupling strength and range parameters, respectively, $N' = \frac{1}{2}(N-1)$ for $N$ odd, and

$$\eta(\alpha) = 2 \sum_{j=1}^{N'} \frac{1}{j^\alpha} \quad (2)$$

is a normalization factor.

In the right hand side of Eq. (1) there is a weighted average of terms involving non-nearest neighbors of each site, $\eta(\alpha)$ being the sum of the corresponding statistical weights. A virtue of this coupling prescription is that the diffusively coupled lattice, where only nearest neighbors are connected, emerges out as a particular case of Eq. (1), when $\alpha \to \infty$. On the other hand, if $\alpha=0$, we recover the global (or "mean-field") coupling, for which all sites interact in the same way regardless of their relative position in the chain. Periodic boundary conditions ($x^{(i)}=x^{(i\pm N)}$) and random initial conditions ($x_0^{(i)}$) will be used throughout this paper.

In CMLs there is typically an interplay between spatial and temporal degrees of freedom. Hence, one is faced with the more difficult problem of characterizing spatiotemporal chaos, whose rigorous definition has been given by Bunimovich and Sinai [30], and relies on a suitable Sinai-Ruelle-Bowen measure, which has been obtained for quite a few cases, such as CMLs of expanding circle maps [31]. Since a rigorous characterization of spatiotemporal chaos is still restricted to such cases, we identify its existence, for practical purposes, by means of two predicates: (i) decay of time correlations, with a nonzero Kolmogorov-Sinai entropy and (ii) decay of spatial correlations over the lattice [32].

The numerical characterization of the latter property can be accomplished, for example, by the analysis of the spatial autocorrelation function. Let us consider, for a fixed time $n$, the average value of the map amplitudes over the entire lat-

tice: $\langle x\rangle_n=(1/N)\Sigma_{i=1}^{N}x_n^{(i)}$. The corresponding deviations from this average are $\hat{x}_n^{(i)}=x_n^{(i)}-\langle x\rangle_n$, such that the spatial autocorrelation function is defined as

$$\mathbf{e}_n(l)\equiv\frac{\frac{1}{N}\sum_{i=1}^{N}\hat{x}_n^{(i)}\hat{x}_n^{(i+l)}}{\frac{1}{N}\sum_{i=1}^{N}(\hat{x}_n^{(i)})^2}, \tag{3}$$

for a given time $n$ and spatial displacement $l=1,2,\ldots$ (notice that, due to the periodic boundary conditions assumed, the spatial displacement is measured in a given ring). It has been found that, for lattices of strongly disordered maps, this correlation decays with the spatial delay $l$ as a power law [32]. In complex patterns formed by spatially ordered and disordered regions, it turns out that $\mathbf{e}(l)$ decays with $l$ in a slower fashion, but without yielding much information about the spatial structure of the pattern [14].

Another possibility is the adaptation of nonlinear time-series diagnostics to investigate spatial randomness at a fixed time [13]. Given a spatial amplitude profile at time $n$, $\{x_n^{(0)},x_n^{(1)},\ldots,x_n^{(N-1)}\}$, we can form an immersion in a $m$-dimensional space, by defining space-separated vectors

$$\vec{\xi}_n^{(i)}=(x_n^{(i)},x_n^{(i+1)},\ldots,x_n^{[i+(m-1)]}), \tag{4}$$

where the spatial separation can be taken as one site and $m$ will be referred to as the embedding dimension.

This procedure has some similarities with the use of time-delay coordinates used to reconstruct the phase space dynamics of a given system from a time series [3]. However, it must be emphasized that the purpose of this construction here is rather distinct, if compared with what is done for a time series. By way of contrast, our main goal using space-separated coordinates is to provide a quantitative characterization of the spatial order and disorder of a complex pattern at a fixed time. While certain measures of roughness turn out to be useful when characterizing spatial patterns, they often fail when the latter consist on more than a single feature. An example readily found in CMLs are patterns composed of smooth domains of different lengths separated by "defects" with spatial disorder. If we try to measure the roughness of this pattern by computing, for instance, the mean square deviation with respect to a spatial average, these inhomogeneities are somewhat overlooked.

The simplest embedding is a two-dimensional spatial return plot of each site amplitude (at a fixed time) $x_n^{(i)}$ versus the amplitude of its nearest neighbor $x_n^{(i+1)}$. In Figs. 1(a)–1(f) we depict a sequence of spatial return plots for the CML (1) with $N=1001$ logistic maps at time $n=5000$. We considered six combinations involving weak (low $\epsilon$) and moderately strong coupling, and an effective range parameter varying from global to local interactions.

If the coupled maps lack spatial correlation, what occurs for weak coupling, even when their dynamics is periodic, the corresponding return plot reveals a cloud of scattered points [Figs. 1(a)–1(c)]. There is an approximate symmetry of the point clouds with respect to the diagonal line $\mathcal{S}$: $x_n^{(i)}=x_n^{(i+1)}$.

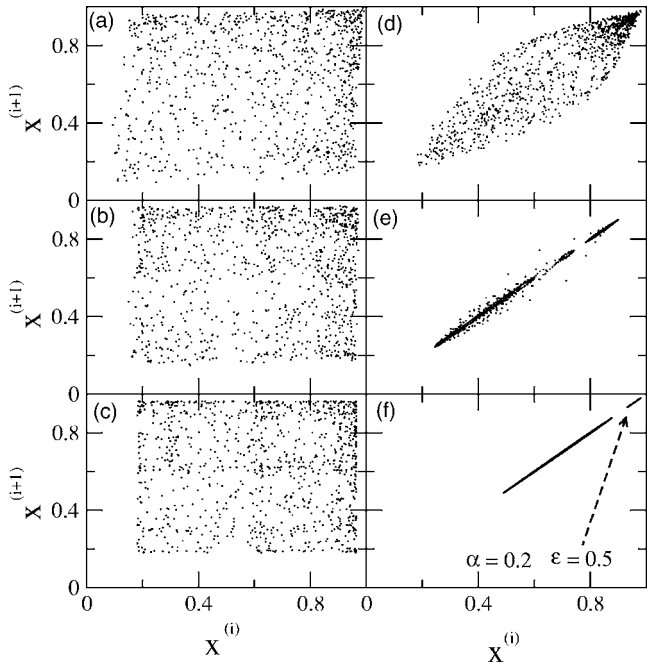


FIG. 1. Spatial return maps for a coupled map lattice (1) with $N=1001$ at a fixed time $n=5000$, and (a) $\alpha=2.0$, $\epsilon=0.1$; (b) $\alpha=1.0$, $\epsilon=0.1$; (c) $\alpha=0.5$, $\epsilon=0.1$; (d) $\alpha=2.0$, $\epsilon=0.5$; (e) $\alpha=1.0$, $\epsilon=0.5$; (f) $\alpha=0.5$, $\epsilon=0.5$ (large plot) and $\alpha=0.2$, $\epsilon=0.5$ (small plot).

When the coupling becomes global (small values of $\alpha$), the overall behavior does not change much, except that the clouds appears to concentrate in a subinterval of $[0,1]$. As we increase the coupling strength $\epsilon$, we see that, even for a local coupling [Fig. 1(d)], there is a concentration of points around $\mathcal{S}$. This means that, while the coupling is rather strong, the spatial pattern is disordered for many different times, what can be grasped in Fig. 2(a), which is an amplitude-space-time plot typical in spatiotemporal chaos scenarios. We remark that, while Figs. 2(a)–2(c) present lattices with a smaller number of sites, for the sake of better visualization, the conclusions drawn here hold also for larger lattices.

If the range parameter $\alpha$ is further decreased towards zero, the coupling between lattice sites becomes more of a global nature, and the cloud of points in the spatial return plot shrinks down to the diagonal line [see Figs. 1(e) and 1(f)]. In terms of the corresponding three-dimensional space-time plots [see Figs. 2(b) and 2(c), respectively] we conclude that, while the temporal evolution of the patterns still seems irregular, the spatial patterns become smoother. Hence, it turns out that spatial return maps are not sufficiently detailed to describe these different types of behavior.

For a very strong coupling the chaotic maps can even synchronize, in the sense that they share the same value of amplitude at each time $n$ within a given interval $x_n^{(1)}=x_n^{(2)}=x_n^{(3)}=\cdots x_n^{(N)}$ [15]. In the case of chaotic synchronized maps, the spatial return plot would reduce to a single point lying on $\mathcal{S}$. We find numerically that this nearly occurs when the coupling range is close to the mean-field case $\alpha=0$, as can be seen in the small diagonal dash at the upper right-hand side of Fig. 1(f).

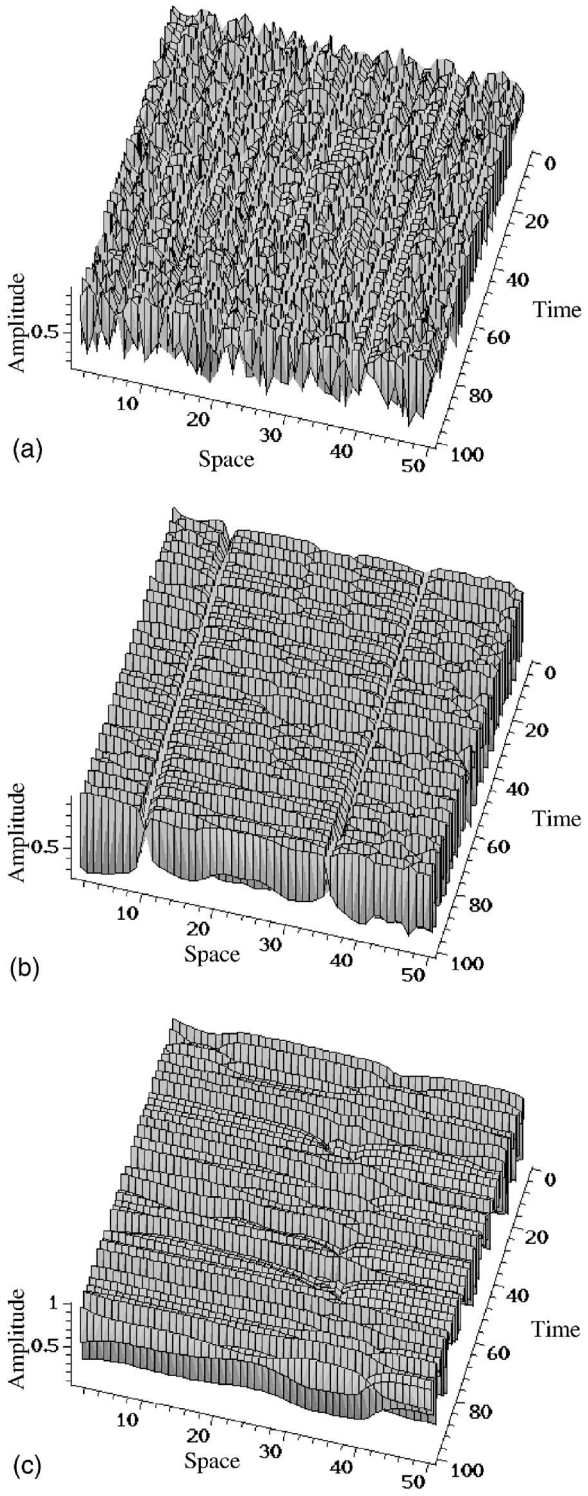


FIG. 2. Space-time-amplitude plots for the CML (1), with $N=51$ sites, $\epsilon=0.5$ and $\alpha=$ (a) 2.0, (b) 1.0, and (c) 0.5.

The point cloud density in the spatial return plot, at a given time $n$, can be numerically computed from a correlation "integral," which involves a summation over all pairs of vectors $\vec{\xi}_n^{(i)}$ belonging to the spatial return plot whose pointwise distance is less than a certain cutoff radius $l$:

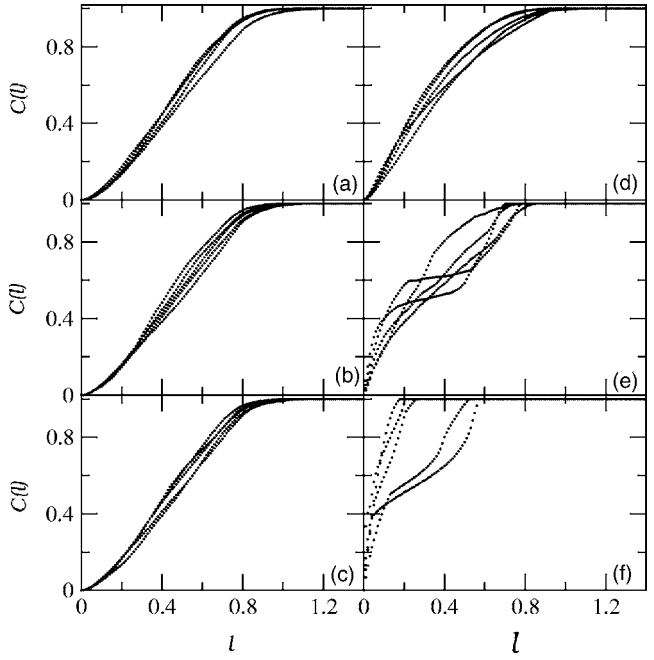


FIG. 3. Spatial correlation integral *versus* radius $l$ for the CML (1) with $N=201$, at a fixed time $n=2000$ and (a) $\alpha=2.0$, $\epsilon=0.1$; (b) $\alpha=1.0$, $\epsilon=0.1$; (c) $\alpha=0.5$, $\epsilon=0.1$; (d) $\alpha=2.0$, $\epsilon=0.5$; (e) $\alpha=1.0$, $\epsilon=0.5$; (f) $\alpha=0.5$, $\epsilon=0.5$.

$$C_n(l) = \lim_{N\to\infty} \frac{1}{N^2} \sum_{i,j=0}^{N-1} \Theta(l - \|\vec{\xi}_n^{(i)} - \vec{\xi}_n^{(j)}\|), \tag{5}$$

where $\|\cdots\|$ is the Euclidean norm and $\Theta$ is the Heaviside unit step function.

Figures 3(a)–3(f) show the dependence of the spatial correlation integral (5) on the cutoff radius $l$ at a fixed time and for three different and randomly chosen initial lattice patterns. The quantity $C_n(l)$ increases with $l$ monotonically from zero (when the cutoff radius vanishes) to unity (when the radius is large enough to engulf the whole point cloud) [Fig. 3(a)]. There is some variation with the initial condition chosen, since we are dealing with patterns exhibiting spatiotemporal chaos, as shown by the space-time-amplitude plot in Fig. 2(a).

When the maps are weakly coupled [Fig. 3(b)], $C_n(l)$ starts to saturate after 0.9 and, as the coupling strength increases [Fig. 3(e) and 3(f)], while the curves reach unity at roughly the same value, there are initial patterns for which the saturation occurs earlier, and this is a consequence of the tendency to synchronization as the coupling strength increases and the range parameter approach values near zero [see also Figs. 2(b) and 2(c)].

We found that, in analogy with time series, the spatial correlation integral also scales with the cutoff radius as a power law $C_n(l) \sim l^{D_2}$, where $D_2$ is the correlation exponent, which can be regarded as a spatial analog of the correlation dimension for the attractor reconstructed through the embedding procedure (note, however, that even in the time domain the algorithm used yields only numerical estimates) [33]. Due to the extensive nature of the CML, the values taken on

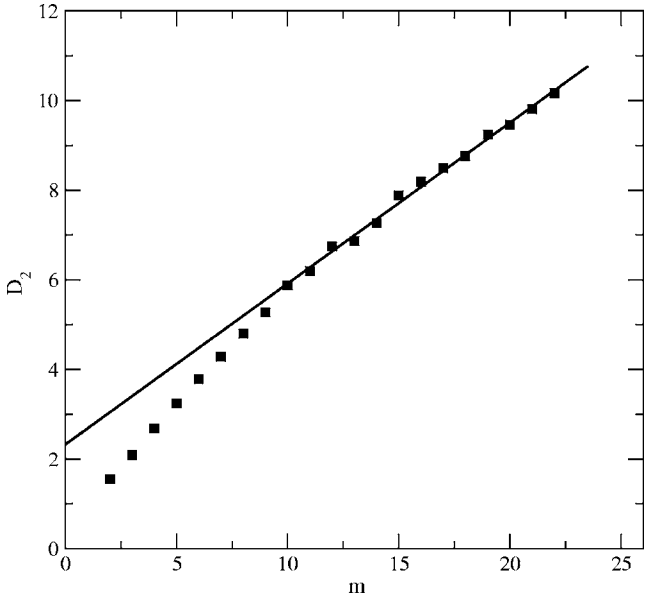


FIG. 4. Spatial correlation exponent as a function of the embedding dimension $m$, for the CML (1) with $N=1001$, at a fixed time $n=2000$, $\alpha=5.0$, and $\epsilon=0.1$. The straight line is a least squares fit with slope equal to the correlation dimension density $d_2=0.36$.

by the exponent $D_2$ increase with the embedding dimension $m$. More significant results can thus be obtained by considering the density of the correlation dimension $d_2=D_2/m$ [13]. The idea of dimension densities has also been found to be very useful in time series from low-dimensional dynamical systems and higher-dimensional spatiotemporal systems [34].

Figure 4 shows the variation of the spatial correlation exponent with the embedding dimension $m$, where we verify a monotonic increase and convergence to a constant value of the correlation dimension density. Accordingly, a least squares fit made after $m\approx 10$ furnishes a density of $d_2=0.36$. This value compares well with the correlation dimension density of $0.30\pm 0.04$ obtained for a quadratic map lattice with a nearest-neighbor but different coupling prescription with respect to ours [13]. This finding supports the view that the second-order Renyi entropy for a lattice, at a fixed time, is an extensive quantity as is the Shannon entropy. The latter measures the information needed to describe the state of the lattice at any fixed time [35]. Thus we can regard $d_2$ as a lower bound for the density of information dimension, as given by the Kaplan-Yorke formula from the spectrum of the Lyapunov dimension [36]. Even though we used different boundary condition, we can assume that the difference between the entropies of the open and the closed systems, at fixed time, would be a constant [13].

## III. SPATIAL RECURRENCE PLOTS

### A. Graphical representation of the spatial recurrence matrix

A promising approach to analyse spatial patterns in complex dynamical systems is based on their recurrence properties. We work with a spatial two-dimensional embedding, using two space-separated coordinates, in such a way to construct a set of vectors $\vec{\xi}_n^{(i)}=(x_n^{(i)},x_n^{(i+1)})$. While the spatial return plot $x_n^{(i)}$ versus $x_n^{(i+1)}$ is a quite direct way to visualize those vectors, it does not tell us too much about the correlation between these vectors, since the information available is limited to the correlation integral $C_n(l)$. To overcome these limits, we propose to analyse the symmetrical $N\times N$ spatial recurrence matrix defined by

$$R_{ij}(l,n)=\Theta(l-\|\vec{\xi}_n^{(i)}-\vec{\xi}_n^{(j)}\|) \tag{6}$$

with entries equal to 0 (1) in the case two points $\vec{\xi}_n^{(i)}=(x_n^{(i)},x_n^{(i+1)})$ and $\vec{\xi}_n^{(j)}=(x_n^{(j)},x_n^{(j+1)})$ are far apart from a distance greater (less) than a cutoff radius $l$. For ordinary differential equations, it was recently shown that ordinary RPs (in time domain) include all dynamical information of a system [6]. On that basis we conjecture that higher order moments of the correlation would be equally present in the SRP, even though we have no rigorous proof for this statement.

The SRP is the graphical representation of the recurrence matrix $R_{ij}(l,n)$ in Eq. (5) for $i,j=0,1,\ldots,N-1$, in the sense that the binary values in $R_{ij}(l,n)$ are represented by a matrix plot with black (white) pixels for entries equal to 1 (0). The spatial correlation integral (5), $C_n(l)=\lim_{N\to\infty}\frac{1}{N^2}\sum_{i,j=0}^{N-1}R_{ij}(l,n)$ is the pointwise density in a SRP, in the same way it does for the point cloud of a spatial return plot [8]. Like in the time domain, SRPs of snapshot patterns (at a fixed time) furnish a qualitative and quantitative characterization of the "sparseness" of the point cloud observed in spatial return plots. Moreover, the presence of regular structures in SRPs is recognized as a fingerprint of spatially correlated clusters of points and thus of smoother spatial patterns.

In Fig. 5 we present a sequence of SRPs obtained for a CML with $\alpha=3.73$ (local coupling) and $\epsilon=1.0$ (strong coupling), at a fixed time and corresponding to different values of the cutoff radius $l$. The horizontal and vertical axes represent, respectively, the indexes $i$ (a site) and $j$ (its lattice-shifted site). A black (white) pixel represents a $(i,j)$ pair for which the pointwise distance is less (more) than $l$ or, in other words, a matrix entry equal to 1 (0). Since the spatial recurrence matrix (6) is symmetric under the $i\to j$ operation, the SRPs are accordingly symmetric with respect to the diagonal line.

For small cutoff radius [Fig. 5(a)] the SRP looks similar to a fractal tapestry, or a Cartesian product of two Cantor-type sets. The correlation integral $C_n(l)$, or the density of black pixels in the SRP, is accordingly low ($\approx 0.094$). Doubling the cutoff radius [Fig. 5(b)] the point cloud becomes denser and the correlation integral is significantly higher ($\approx 0.28$). The density of the point cloud in the SRP increases with the cutoff radius, as illustrated by Figs. 5(c), for which $C_n(l=0.4)=0.65$; 5(d), where $C_n(l=0.6)=0.91$; and $C_n(l=0.8)=0.99$ in Fig. 5(e). In the last case [Fig. 5(f)] the SRP becomes entirely filled up, reflecting the saturation existing for large cutoff radius, such that the correlation integral reaches unity. These results are in agreement with the monotonic increase of the spatial correlation integral shown

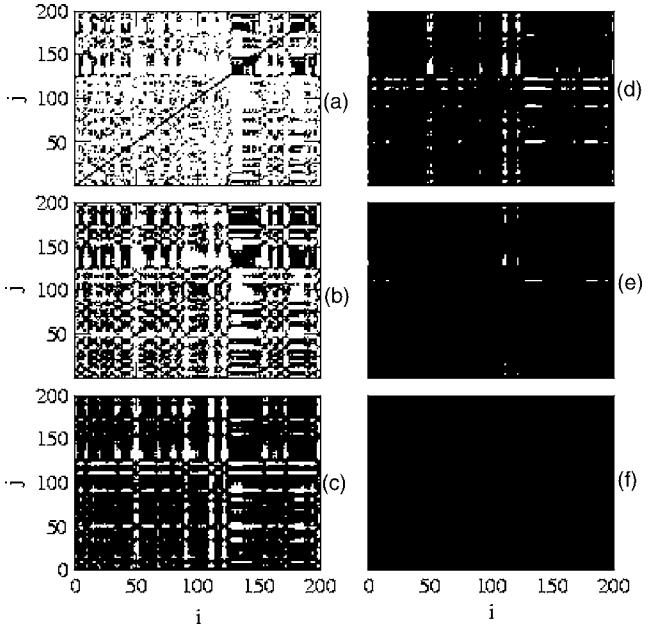


FIG. 5. Spatial recurrence plots for different values of the cutoff radius for the CML (1) with $N=201$, $\alpha=3.73$, $\epsilon=1.0$, $n=2000$ and (a) $l=0.1$, (b) $l=0.2$, (c) $l=0.4$, (d) $l=0.6$, (e) $l=0.8$, (f) $l=1.0$.

by Fig. 3. Since Figs. 5(c)–5(f), obtained for quite large cutoff radii, are so densely filled that we barely distinguish possibly existent structures, we shall use small cutoff radii, similar to $l=0.1$, in the forthcoming analyses.

The dependence of the SRPs on the coupling parameters is depicted in Fig. 6. As a general trend, for a fixed cutoff radius, the recurrence plot becomes denser as the coupling effect is more intense, both by increasing the coupling

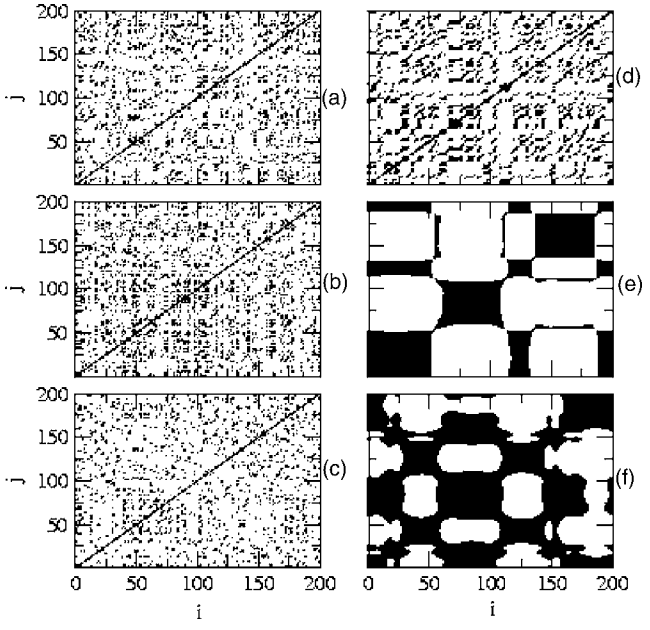


FIG. 6. Spatial recurrence plots for the following $(\alpha,\epsilon)$ values in the coupling parameter space: (a) (2.0,0.1), (b) (1.0,0.1), (c) (0.5,0.1), (d) (2.0,0.5), (e) (1.0,0.5), (f) (0.5,0.5). We used a cutoff radius $l=0.1$ and $N=201$.

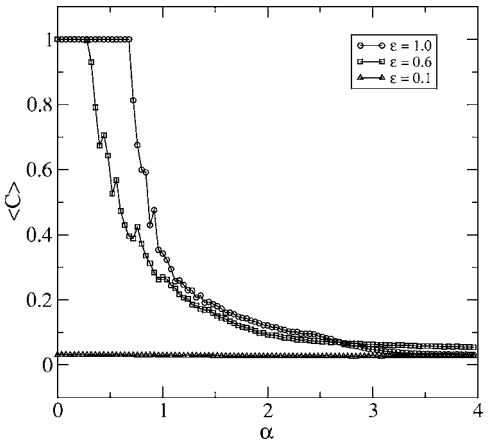


FIG. 7. Average spatial correlation integral *versus* the range parameter for different coupling strengths. We used a cutoff radius $l=0.1$ and $N=201$.

strength $\epsilon$ or diminishing the range parameter $\alpha$. If we take a weak coupling ($\epsilon=0.1$) and vary the $\alpha$ parameter [Figs. 6(a)–6(c)] little effect is seen in the SRP, indicating a sparse distribution of iterates in the spatial return plot. In fact, the values of the correlation integral vary from 0.058 to 0.047 as $\alpha$ goes from 2.0 [Fig. 6(a)] to 0.5 [Fig. 6(c)]. By way of contrast, when performing the same kind of test with a stronger coupling (e.g., $\epsilon=0.5$), we see a denser distribution of points with correlation integral varying from 0.11 [Fig. 6(d)], to 0.29 [Fig. 6(e)], and 0.49 [Fig. 6(f)], as the range parameter decreases from a local to a global type of coupling. We can also observe in Figs. 6(e) and 6(f) a pronounced tendency of formation of checkerboard-type patterns in SRPs, what suggests the existence of domains with high degree of spatial coherence.

The results shown in Fig. 3 indicate that the actual value of $C_n(l)$ depends also on the initial conditions chosen, and so we make an average over a number $N_0$ of randomly chosen initial conditions $\langle C_n(l)\rangle=(1/N_0)\Sigma_k C_n(l,x_{0k}^{(i)})$. Figure 7 presents the dependence of the average correlation integral with the coupling range parameter $\alpha$, for some representative values of the coupling strength $\epsilon$. For weak coupling (e.g., $\epsilon=0.1$) the values of $\langle C_n(l)\rangle$ are close to zero and practically independent of $\alpha$. In fact, weakly coupled lattices of chaotic maps typically present a noncoherent (nonsynchronized) behavior, regardless of the coupling range. This is reflected in the sparseness of points of the corresponding SRPs [see also Figs. 6(a)–6(c)] and in the low values that $\langle C_n(l)\rangle$ assumes for these cases.

Higher values of $\epsilon$ are expected to yield synchronized patterns, though, what can be seen in the plateau of high $\langle C_n(l)\rangle$ values existent when the range parameter $\alpha$ is low enough. In such cases, a sharp transition between completely synchronized and nonsynchronized regimes occurs for $\alpha$ values usually less than unity [see also Figs. 6(d)–6(f)]. If $\alpha$ is too large, however, the locally coupled lattice does not synchronize at all, even if $\epsilon$ takes on larger values, and the corresponding SRPs would be so sparse as those obtained for low $\epsilon$. The information on the synchronized behavior displayed by the average correlation integral agrees with other

numerical diagnostics (e.g., Kuramoto's order parameter) used in earlier works on synchronization of chaos in CMLs of the type given by Eq. (1) [37].

### B. Measures of complexity in a spatial recurrence plot

Another quantitative characterization of SRPs is based on a detailed analysis of the large and small-scale patterns or structures: (i) diagonal structures which reflect similar local behavior of different parts of the spatial pattern [2,9,38], (ii) vertical structures (black lines) represent patterns which do not change along the lattice, e.g., as it typically happens in intermittency [7,39]. Horizontal structures are equally useful in symmetric recurrence plots, such that it suffices to consider those vertical structures found in SRPs.

Vertical structures at a given time $n$ can formally be considered as sequences of black pixels $R_{ij}(l,n)$ such that, for a $k$th vertical structure the inequality

$$R_{i,k}(l,n)R_{i,k+1}(l,n) + R_{i,k}(l,n)R_{i,k-1}(l,n) > 0 \tag{7}$$

holds for the corresponding value of $i$ [7]. The number of black pixels in the $k$th vertical structure will be denoted as $v_k$. A glance at some sparse recurrence plot, say Fig. 5(a), shows that there are typically many vertical structures in such a way that a frequency distribution $P(v_k)$ can be drawn from all lines of a given SRP. We shall take $v_{\min}=2$ as the minimum length of a vertical structure.

Vertical structures represent highly correlated strings of points in the SRP, and thus their appearance signals the existence of spatially coherent sites in the CML. In particular, completely synchronized states, for which the state variables share a same value as the time evolves, are extreme examples of spatially coherent states. Synchronized states in CMLs may span the entire lattice or either form a plateau, depending on the individual dynamical behavior of each map, as well as the values of the coupling parameters. Thus, we expect the formation of many vertical structures in a CML which has a number of synchronization plateaus. However, it must be stressed that the converse is not necessarily true: the sheer existence of vertical structures does not imply the existence of a same number of synchronization plateaus, but only that the sites are correlated enough to be within a distance $l$ in the reconstructed space. We claim that, as the cutoff radius $l$ tends to zero, the existence of vertical structures in a SRP implies the appearance of synchronization plateaus in the CML and vice versa.

Marwan and co-workers [7] have defined the laminarity $\Lambda$ of a recurrence plot as the ratio between the number of pixels belonging to vertical structures and the total number of pixels of the SRP

$$\Lambda = \frac{\sum_{v_k \geq 2} v_k P(v_k)}{\sum_{\text{all } k} v_k P(v_k)}, \tag{8}$$

which represents the relative number of points forming vertical structures, regardless of the lengths of each individual structure. In order to get the latter information, it is useful to compute the average length $L$ of vertical structures in the recurrence plots (or "trapping length," in analogy with the word coined for time series):

$$L = \frac{\sum_{v_k \geq 2} v_k P(v_k)}{\sum_{v_k \geq 2} P(v_k)}. \tag{9}$$

The total number of vertical structures in a CML of $N$ sites may vary between unity and $N/v_{\min}=N/2$. While the former case would represent a completely synchronized lattice, the latter is usually not realized in CMLs. A completely nonsynchronized lattice would have few vertical structures, if any (which are possible for a cutoff radius large enough). Hence, a completely synchronized state has $\Lambda_{\max}=1$ for any cutoff radius $l$ but, if $l$ is not necessarily small, the converse is not true in general. The smallest possible value of the laminarity is $\Lambda_{\min}=0$, in the case we do not have any vertical structures at all. However, even if the lattice has the smallest possible number of vertical structures, we still would have $\Lambda=(N/2)/(N^2)=1/(2N)$, which goes to zero as $N\to\infty$. Hence, for nonsynchronized patterns $\Lambda$ takes on a small yet nonzero value.

The trapping length seems similar to the laminarity but conveys a different information: let us consider, for example, a SRP with more single pixels than vertical structures. In this case, even if there are many vertical structures (what would give a quite large laminarity), their proportion relative to the isolated points ($v_k<2$) is small, and accordingly the trapping length can be significantly lower than the laminarity. On the other hand, if the laminarity is small, the corresponding trapping length can be comparatively large if the few vertical structures have an individually large number of pixels. In fact, the trapping length for a completely synchronized lattice takes on its maximum value $L_{\max}=1.0$. On the other hand, a nonsynchronized state with no vertical structures whatsoever would have $L_{\min}=0$ for any cutoff radius $l$. Since, for nonzero cutoff radius, we can have some degree of spatial coherence even for nonsynchronized maps, we expect $L_{\min}$ to reach small but nonzero values again.

The average laminarity $\langle\Lambda\rangle$, taken with respect to a number of different and randomly chosen initial patterns, is shown in Fig. 8 as a function of the range parameter for some representative values of the coupling strength. The results confirm the information obtained from Fig. 7, for low-$\epsilon$ values yield sparse SRPs, since the corresponding laminarity indicates that vertical structures are comparatively rare. Many vertical structures can be found at values of coupling strength for which the lattice can synchronize, and, accordingly, the laminarity achieves its maximum value of unity. Curiously, intermediate values of $\epsilon$ may give an abundance of vertical structures even when higher $\epsilon$ values do not. This indicates the emergence of a number of spatially coherent structures, within the cutoff radius ($l=0.1$) chosen, other than synchronization plateaus.

Our results for the trapping length, as a function of the range parameter, are depicted in Fig. 9. There are some similarities between the information conveyed by laminarity and trapping length: for weak coupling both $\langle\Lambda\rangle$ and $\langle L\rangle$ are low,

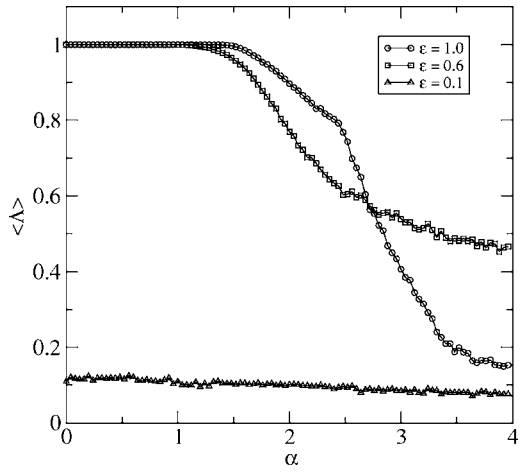


FIG. 8. Average laminarity *versus* the range parameter for different coupling strengths. We used a cutoff radius $l=0.1$ and $N=201$.

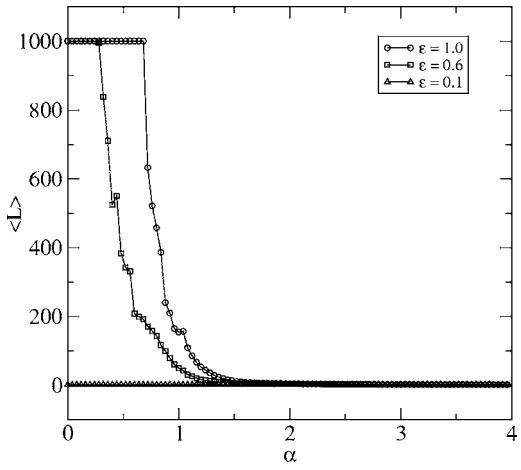


FIG. 9. Average trapping length *versus* the range parameter for different coupling strengths. We used a cutoff radius $l=0.1$ and $N=201$.

thanks to the sparseness of the plots; and the combination of $\alpha$ small and strong coupling leads to saturation of both quantities. However, as already expected, there are quantitative differences, especially for the large-$\alpha$ case. Whereas the laminarity decreases very slowly, the trapping length goes to zero in a steep fashion, indicating that the corresponding SRPs have many vertical structures with a small number of pixels, a fact that can be checked out by glancing at Fig. 6, for example.

In order to demonstrate the usefulness of SRPs and the numerical diagnostics of spatial complexity here introduced, we show in Fig. 10(a) the spatial pattern (at a fixed time $n=2001$) obtained for a lattice with $N=1001$ sites, and coupling parameters $\alpha=2.0$, $\epsilon=1.0$, and the corresponding SRP obtained from a smaller cutoff radius $l=0.05$ for better graphical resolution. The existence of a large number of plateaus or near-plateaus of synchronized behavior manifests itself in a large number of wide vertical structures. Indeed, the spatial correlation integral, laminarity, and trapping length take on the values $R=0.175$, $\Lambda=0.886$, and $L=5.24$, respectively. Figure 10(b) depicts a similar lattice with all parameters kept fixed but the range parameter, which is now $\alpha=2.8$. This slight change is already enough to change the spatial pattern for both the number and the widths of vertical structures decrease, and the overall pattern seems more noisy than before. In fact, the numerical diagnostics we introduced here exhibit lower values, namely, $R=0.129$, $\Lambda=0.569$, and $L=3.19$.

Moreover, such a difference in the spatial patterns is practically not detected by standard measures of spatial complexity, such as the rugosity (r.m.s. of height fluctuations) and the autocorrelation function given by Eq. (3). Indeed, the rugosity for the pattern depicted in Figs. 10(a) and 10(b) are $w=0.216$ and 0.246, respectively. This is also the case with the autocorrelation function, whose dependence on the spatial delay $l$ is shown in Fig. 11 for the two patterns exhibited in Fig. 10. There is a similar linear decay for both patterns, presenting nearly the same slope and with the same value of $l=9$ sites for the vanishing of the autocorrelation. Hence, SRPs can be more effective to distinguish and quantify the complexity of such spatial patterns.

Some remarks are in order here, with respect to the numerical diagnostics of spatial disorder for SRP. The correlation integral, being just a density of points, does not take into account fine structures of the point cloud distribution in a SRP. One possible approach would be to consider higher moments of this point density with respect to the diagonal line; e.g., an average quadratic distance to the diagonal line

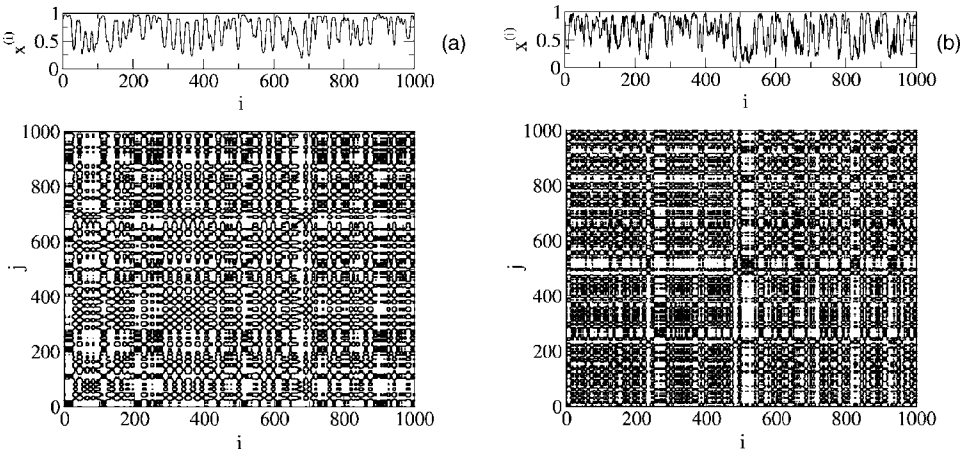


FIG. 10. Spatial pattern (at a fixed time $n=2001$) and the corresponding SRP (cutoff radius $l=0.05$) obtained for a lattice with $N=1001$ sites, and coupling parameters $\epsilon=1.0$, and (a) $\alpha=2.0$ and (b) $\alpha=2.8$.

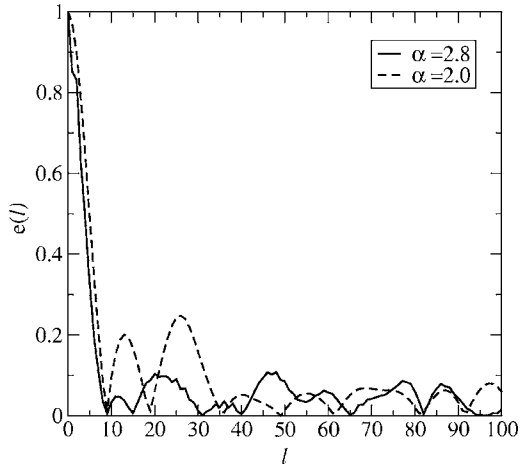


FIG. 11. Spatial autocorrelation function versus spatial delay (measured in number of lattice sites) for the two patterns considered in Fig. 10.

or a typical "width" of the point cloud, assuming it is symmetric with respect to the diagonal line. Other line of thought, and which has been pursued in this work, considers the structures directly observed in the SRPs, and seems to be more fruitful in the ensuing analyses.

Very disordered spatial patterns, like those seen in CMLs for weak coupling, are well described by both the correlation integral and the laminarity. It is actually for complex patterns, for which disordered regions coexist with smoother ones, where the laminarity of the corresponding SRPs shows its usefulness. Let us compare, for instance, Figs. 7 and 8, for which both curves, in the case of higher $\epsilon$ values, are quite different. The correlation integral decays with increasing $\alpha$ in a more abrupt way, resembling a phase transition occurring at a specific critical value of $\alpha$. The laminarity, on the other hand, decays in a slower fashion, showing that the increasing complexity of the patterns, which implies in more vertical (or horizontal) structures, is best described by this quantity. The trapping length, on its hand, is useful to distinguish spatial patterns with abundance of noncorrelated sites from patterns with a large number of short highly correlated pieces. This distinction is specially important for large lattices.

## IV. CONCLUSIONS

In order to give a graphical representation of the spatial correlation matrix, we introduced spatial recurrence plots (SRP) as numerical tools for identification of spatially coherent patterns at a fixed time. We used coupled map lattices (CML) as prototypical examples of complex spatiotemporal patterns. The recurrences were computed in a two-dimensional reconstructed space, whose coordinates are obtained through spatial separations. A density of spatial correlation integral can be obtained in this way, and it scales with the number of separated lattice sites as a power law, whose slope is the density of correlation dimension. The SRP reveals to be a good visual diagnostic of the spatial patterns obtained from the CML, such as synchronized states and other spatially coherent structures similar to domains. The measures of complexity, laminarity and trapping length, obtained from the SRP, enable us to elucidate the role of the vertical structures and single pixels.

Although we have restricted ourselves in this paper to a specific CML as a paradigm system, the SRP concept is far reaching in the sense that it can be applied to any spatial profile. One example from condensed matter physics would be a snapshot rugosity profile of a given sample of metallic film: a SRP could be used, in such a case, to provide an alternative characterization of spatial disorder and how it would change by varying some external condition, like the attack of chemicals [40]. Spatial recurrence plots can also provide a systematic way to study spatiotemporal patterns in CMLs and other spatially extended systems, such as chains of coupled oscillators and partial differential equations [41]. More specifically, the numerical results presented in this paper can be used to investigate spatially extended systems for which the effective interaction range is a key feature, as in reaction-diffusion systems where there is a rapidly diffusing component mediating the interactions through long distances [42,43].

Using a coupled map or a continuous-time oscillator lattice is a natural choice for constructing SRPs, since the spatial variable is already discretized in unit steps, so facilitating the obtention of spatial return plots. However, other spatially extended systems can also be investigated through the method we have proposed in this paper. For example, consider a homogeneous and periodically driven reaction-diffusion equation [44] $x_t = Dx_{yy} + R(x)\Sigma_k \delta(t - k\tau)$, where $x(y,t)$ is some scalar field, $y$ is position, $t$ is time, $D$ is a diffusion constant, and $R(x) \equiv f(x) - x$ is a nonlinear reaction rate. The impulsive character of the time-periodic reaction term enables us to discretize both the space and time variables so as to obtain a locally coupled map lattice of the form (1), when $\alpha \to \infty$.

Time is discretized from integrating the partial differential equation in the neighborhood of each $\delta$-function kick, at $t = n\tau$, whereas space is discretized through introducing a lattice parameter $w$, such that $y = iw$, $i$ a positive integer. The coupling term in the resulting coupled map lattice will be thus the discretized form of the second spatial derivative. If we keep the time as a continuous variable, the resulting system would be a chain of continuous-time coupled oscillators, similar to a lattice of coupled Rössler chaotic systems [45]; but the key ingredient, which is the lattice structure, would remain the same as before. Even though we are faced with other classes of partial differential equations, standard techniques of numerical differentiation (cf. [46]) allow us to discretize space so that the lattice parameter can be normalized to unity.

A further step would be to consider the extension of the SRPs for running times. Since each map has its own dynamics, there are as time series as maps in the lattice, with SRPs as their corresponding snapshots at discrete times. Due to the large dimensionality of data arrays produced with even a few coupled systems, a discussion similar to that presented in this paper would have to employ statistical characterization such as, e.g., cross-correlation data analysis and bispectral techniques. The application of standard statistical techniques to higher-dimensional recurrence plots thus poses stimulant challenges.

**ACKNOWLEDGMENTS**

This work was made possible with partial financial help from CNPq and CAPES (Brazilian Government Agencies). The numerical computations were performed using the NAUTILUS cluster at UFPR. J.K. is thankful for the financial support from SFB 555 (DFG) and E2-C2 (EC). R.L.V. acknowledges useful discussions and suggestions from M. Thiel, M. C. Romano, and N. Marwan.

[1] J. P. Eckmann, S. O. Kamphorst, and D. Ruelle, Europhys. Lett. **4**, 963 (1987).
[2] M. Casdagli, Physica D **108**, 12 (1997).
[3] H. Kantz and T. Schreiber, *Nonlinear Time Series Analysis* (Cambridge University Press, Cambridge, 1997).
[4] M. Koebbe and G. Mayer-Kress, in *Nonlinear Modeling and Forecasting*, edited by M. Casdagli and S. Eubank (Addison-Wesley, Reading, MA, 1991), pp. 361–378.
[5] F. M. Atay and Y. Altintas, Phys. Rev. E **59**, 6593 (1999).
[6] M. Thiel, M. Romano, and J. Kurths, Phys. Lett. A **330**, 343 (2004).
[7] N. Marwan, N. Wessel, U. Meyerfeldt, A. Schirdewan, and J. Kurths, Phys. Rev. E **66**, 026702 (2002).
[8] M. Thiel, M. C. Romano, P. Read, and J. Kurths, Chaos **14**, 234 (2004).
[9] J. P. Zbilut and C. L. Webber, Jr., Phys. Lett. A **171**, 199 (1992).
[10] L. Matassini, H. Kantz, J. Holyst, and R. Hegger, Phys. Rev. E **65**, 021102 (2002).
[11] M. Thiel, M. C. Romano, J. Kurths, R. Meucci, E. Allaria, and T. Arecchi, Physica D **171**, 138 (2003).
[12] R. Badii and A. Politi, *Complexity: Hierarchical Structures and Scaling in Physics* (Cambridge University Press, Cambridge, 1997).
[13] P. Grassberger, Phys. Scr. **40**, 346 (1989).
[14] D. B. Vasconcelos, R. L. Viana, S. R. Lopes, A. M. Batista, and S. E. de S. Pinto, Physica A **343**, 201 (2004).
[15] A. Pikovsky, M. Rosenblum, and J. Kurths, *Synchronization: A Universal Concept in Nonlinear Science* (Cambridge University Press, Cambridge, 2000).
[16] F. Takens, in *Dynamical Systems and Turbulence*, edited by D. A. Rand and L. S. Young, Vol. 898 of *Springer Lecture Notes in Mathematics* (Springer-Verlag, New York, 1980).
[17] S. Sinha, Phys. Lett. A **245**, 393 (1998).
[18] A. L. Barabási and H. E. Stanley, *Fractal Concepts in Surface Growth* (Cambridge University Press, Cambridge, 1995).
[19] B. B. Mandelbrot, D. E. Passoja, and A. J. Paullay, Nature (London) **308**, 721 (1984).
[20] E. Bouchaud, G. Lapasset, and J. Planés, Europhys. Lett. **13**, 73 (1990); J. Krim and J. O. Indekeu, Phys. Rev. E **48**, 1576 (1993).
[21] M. Kardar, G. Parisi, and Y.-C. Zhang, Phys. Rev. Lett. **56**, 889 (1986).
[22] G. W. Baxter, R. P. Behringer, T. Fagert, and G. A. Johnson, Phys. Rev. Lett. **62**, 2825 (1989).
[23] J. Hohaus, H.-U. Schreiber, and U. Rder, Electrochem. Solid-State Lett. **3**, 147 (2000).
[24] Y. Braiman, H. G. E. Hentschel, F. Family, C. Mak, and J. Krim, Phys. Rev. E **59**, R4737 (1999).
[25] K. B. Briggs, D. R. Jackson, and S. Stanic, J. Acoust. Soc. Am. **105**, 1079 (1999).
[26] K. Kaneko, in *Theory and Applications of Coupled Map Lattices*, edited by K. Kaneko (Wiley, Chichester, 1993).
[27] J. P. Crutchfield and K. Kaneko, in *Directions in Chaos*, edited by Hao Bai-lin (World Scientific, Singapore, 1987), Vol. 1.
[28] K. Kaneko, Physica D **23**, 436 (1986).
[29] S. E. de S. Pinto and R. L. Viana, Phys. Rev. E **61**, 5154 (2000).
[30] L. A. Bunimovich and Ya. G. Sinai, Nonlinearity **1**, 491 (1988).
[31] M. Jiang and Y. B. Pesin, Commun. Math. Phys. **193**, 675 (1998).
[32] J. M. Houlrik and M. H. Jensen, Phys. Lett. A **163**, 275 (1992).
[33] P. Grassberger and I. Procaccia, Physica D **9**, 189 (1983).
[34] C. Raab and J. Kurths, Phys. Rev. E **64**, 016216 (2001).
[35] P. Cipriani and A. Politi, J. Stat. Phys. **114**, 205 (2004).
[36] A. M. Batista, S. E. de S. Pinto, R. L. Viana, and S. R. Lopes, Phys. Rev. E **65**, 056209 (2002).
[37] R. L. Viana, C. Grebogi, S. E. de S. Pinto, S. R. Lopes, A. M. Batista, and J. Kurths, Phys. Rev. E **68**, 067204 (2003); C. Anteneodo, S. E. S. Pinto, A. M. Batista, and R. L. Viana, *ibid.* **68**, 045202(R) (2003); C. Anteneodo, A. M. Batista, and R. L. Viana, Phys. Lett. A **326**, 227 (2004).
[38] L. L. Trulla, A. Giuliani, J. P. Zbilut, and C. L. Webber, Jr., Phys. Lett. A **223**, 255 (1996).
[39] N. Marwan and J. Kurths, Phys. Lett. A **302**, 299 (2002).
[40] A. Ungersbock and B. Rahn, J. Mater. Sci.: Mater. Med. **5**, 434 (1994).
[41] K. Kaneko, Physica D **34**, 1 (1989).
[42] Y. Kuramoto and H. Nakao, Physica D **103**, 294 (1997).
[43] Y. Kuramoto, D. Battogtokh, and H. Nakao, Phys. Rev. Lett. **81**, 3543 (1998).
[44] A. J. Lichtenberg and M. A. Lieberman, *Regular and Chaotic Motion*, 2nd ed. (Springer Verlag, New York, 1992).
[45] J. F. Heagy, T. L. Carroll, and L. M. Pecora, Phys. Rev. E **50**, 1874 (1994); Gang Hu, Ying Zhang, H. A. Cerdeira, and Shigang Chen, Phys. Rev. Lett. **85**, 3377 (2000).
[46] W. H. Press, S. A. Teukolsky, W. T. Wetterling, and B. P. Flannery, *Numerical Recipes in FORTRAN: The Art of Scientific Computing*, 2nd ed. (Cambridge University Press, Cambridge, 1992), pp. 180.